Evaluation of New 3-Mercaptopropionate Thiols for Thiol-ene Photopolymerization Coatings Using Experimental Design

Kosin Wutticharoenwong, Mark D. Soucek

Department of Polymer Engineering, The University of Akron, Akron, Ohio 44325

Received 7 July 2008; accepted 4 November 2008
DOI 10.1002/app.29796
Published online 27 April 2009 in Wiley InterScience (www.interscience.wiley.com).

ABSTRACT: Three 3-mercaptopropionate thiols, 1,6-Hexane bis(3-mercaptopropionate) (HD-SH), *trans*-1,4-Cyclohexanedimethyl bis(3-mercaptopropionate) (CHDM-SH), and 4,4′-Isopropylidenedicyclohexane bis(3-mercaptopropionate) (HBPA-SH) were formulated with 1,3,5-triallyl-1,3,5-triazine-2,4,6(1*H*,3*H*,5*H*)-trione (TATATO) and photoinitiator. The formulations were photopolymerized via thiol-ene photopolymerization. A ternary experimental design was employed to elucidate the influence the three thiols on the thermomechanical and coatings properties of thiol-ene photopolymerizable materials. Tensile strength, tensile modulus, elongation-to-break, glass transition temperature (T_g), and crosslink density (XLD) were investigated. Coating properties including pencil hardness, pull-off adhesion, MEK double rubs, and gloss were also investigated. Relative reaction conversion was determined by photo differential scanning calorimeter (PDSC). Thiol-ene photopolymerizable materials containing HBPA-SH resulted in improving tensile strength, tensile modulus, T_g, and pencil hardness but lowering of crosslink density and relative conversion. This was attributed to steric and rigidity of the double cycloaliphatic structure. The inclusion of CHDM-SH into the systems resulted in the synergistic effect on elongation-to-break and pull-off adhesion. The HD-SH generally resulted in a diminution of thermomechanical and coating properties, but improved the crosslink density. © 2009 Wiley Periodicals, Inc. J Appl Polym Sci 113: 2173–2185, 2009

Key words: coatings; crosslinking; curing of polymers; photopolymerization

INTRODUCTION

The overall thiol-ene photopolymerization reaction is represented in Scheme 1. Recently, Thiol-ene photopolymerization has been an attractive area over the past few years due to the fast growing in the field photopolymerization and the special characteristics of thiol-ene reaction.[1–3] Thiol-ene photopolymerization exhibits a number of advantages over conventional UV-curable resins including inherently rapid reaction rate, reduced oxygen inhibition, reduced film shrinkage problem, and good film-substrate adhesion properties.[4–7]

An important advantage of thiol-ene photopolymerization is that thiol-ene photopolymerization can proceed in the presence of oxygen.[8] Conventional free radical polymerization in the presence of oxygen leads to a formation of peroxide, which slows the curing mechanism down to a termination of the reactive free radical. Conversely, thiol-ene photopolymerization incorporates oxygen into the growing chain of polymer as peroxy radical. Peroxy radical can proceed chain transfer with a thiol to produce a new thiyl radical, which can continue the polymerization reaction. In other words, the thiol-ene polymerization reaction can tolerate oxygen without slowing the overall reaction rate, which is in contrast to the acrylate-based systems. Nevertheless, one of the current disadvantages of thiol-ene material is that hardness, high glass transition temperature, and toughness are not easily obtainable. This is the result of the flexible thioether linkages within the thiol-ene crosslinked network structure.

Recently, thiol-acrylate photopolymerization has been found to be tunable by the concentration of acrylate used. The glass transition temperature and hardness were variable dependent on the concentration of acrylate.[9] However, the present choices of available alkene/acrylate systems limit the potential for selectively altering physical, mechanical, and optical properties. A solution to this problem can be obtained by developing new thiols. Unfortunately, synthetic attempts of new thiols for thiol-ene photopolymerization have only been recently reported.[10]

Another approach to develop hard thiol-ene polymers is to utilize thiol and ene monomer with rigid structure. However, synthesis of new monomer is necessary because of limited availability of rigid thiol and alkene structures that are not

Correspondence to: M. D. Soucek (msoucek@uakron.edu).

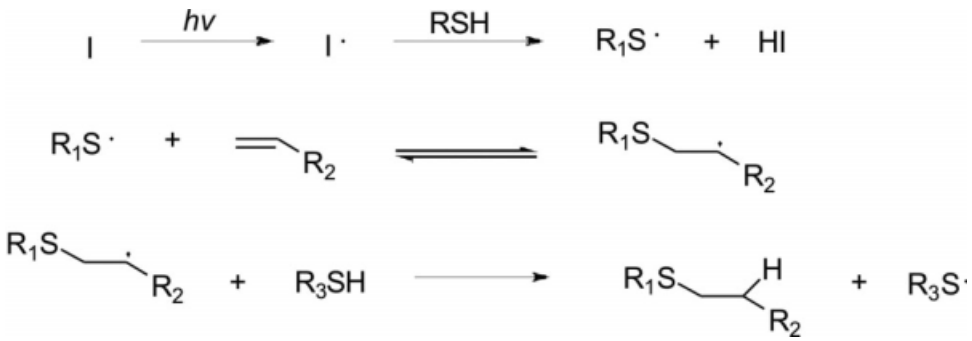

Scheme 1 Thiol-ene photopolymerization reaction.

homopolymerizable. Ternary systems of thiol-vinyl-vinyl were studied to compare to binary thiol-ene system. The extent of vinyl homopolymerization and the thiyl radical reactivity toward both vinyl groups determine the polymerization mechanism and network evolution of the ternary systems. Control of polymerization kinetics, crosslinked network structure, and mechanical properties can be achieved with the thiol-vinyl-vinyl ternary system. Evaluation of thiol-allyl ether-methacrylate ternary systems showed that the concentration and structure of the thiol significantly affect the polymerization processes and network structure.[11]

Investigation of film and coatings properties of thiol-ene photopolymerization can be relatively difficult because of the complexity and number of variable. Simple experiment can take long times to understand complex systems. Design of experiments can elucidate and quantify how the interaction of two or more factors affects the system. It is also easier with the designed experiments to demonstrate nonlinear relationships. The object of the response surface methodology (RSM) is to form a mathematical model of the system by using statistical analysis of the experimental results. When nonlinearity is concerned, more than two level experiments are required to describe a response curve.[12] In a mixture experiment, a special type of response surface experiment, the factors are the ingredients or components of a mixture. The response is a function of the proportions of each ingredient. These proportional amounts of each ingredient are typically measured by weight, by volume, by mole ratio, and so forth. Data obtained from the designed experiments can be analyzed using analysis of variance (ANOVA), a collection of statistical models that compares means by subdividing the overall observed variance into different parts. ANOVA shows whether model variance is significant when compared with experimental variances.

In this study, thiol-ene photopolymerization materials were statistically investigated on the variation of thiol chemical structures. Three UV-curable mercaptopropionate thiols, 1,6-Hexane bis(3-mercaptopropionate) (HD-SH), *trans*-1,4-Cyclohexanedimethyl bis(3-mercaptopropionate) (CHDM-SH), and 4,4′-Isopropylidenedicyclohexane bis(3-mercaptopropionate) (HBPA-SH) were statistically formulated with 1,3,5-triallyl-1,3,5-triazine-2,4,6(1*H*,3*H*,5*H*)-trione (TATATO) for the elucidation of dependent variables, and optimization of mechanical, thermal, and coatings properties. The mechanical and thermal properties were evaluated via stress–strain tensile experiments and dynamic mechanical analysis (DMA). Pencil hardness, pull-off adhesion, MEK double rubs, and gloss test were performed to investigate the coatings properties. Relative reaction conversion was determined by differential scanning calorimetry method. The variables were evaluated through experimental design via a simplex centroid model.

EXPERIMENTAL

Materials

4,4′-*Iso*propylidenedicyclohexanol mixture of isomers (hydrogenated Bisphenol-A) (HBPA), 1,6-hexanediol (HD), *trans*-1,4-bis(hydroxymethyl)cyclohexane (CHDM) 3-mercaptopropionic acid, *p*-toluenesulfonic acid (*p*-TSA), toluene (reagent grade), diethyl ether anhydrous, 1,3,5-Triallyl-1,3,5-triazine-2,4,6(1*H*,3*H*,5*H*)-trione (TATATO), and magnesium sulfate was purchased from Aldrich Chemical company. The photoinitiator 2,2-dimethyl-2-hydroxyacetophenone (Darocure 1173) was obtained from Ciba Specialty. All the chemicals were used as received. The chemical structure of the photoinitiator is shown in Figure 1.

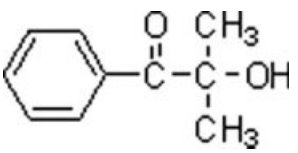

Figure 1 Chemical formula of 2,2-dimethly-2-hydroxyacetophenone (Darocure 1173).

Synthesis of the thiols

The synthesis of thiols: (1) 1,6-Hexane bis(3-mercaptopropionate) (HD-SH), (2) *trans*-1,4-Cyclohexanedimethyl bis(3-mercaptopropionate) (CHDM-SH), and (3) 4,4′-isopropylidenedicyclohexane bis(3-mercaptopropionate) (HBPA-SH) was accomplished according to the previous literatures.[10] All the spectroscopic identification was consistent with the previously reported literature.[10]

1,6-Hexane bis(3-mercaptopropionate)

1,6-Hexanediol (10.78 g, 0.091 mol), 3-mercaptopropionic acid (22.32 g, 0.210 mol), and *p*-Toluenesulfonic acid (0.2 g, 0.001mol) were dissolved in toluene (150 mL) and charged into a 500-mL round-bottom three-necked flask equipped with mechanical stirrer, Dean-Stark trap, and reflux condenser. The mixture was purged with argon, and heated to reflux temperature $\sim$ 110°C. The mixture was kept at reflux temperature for 3 h to ensure completed reaction after which the toluene was removed from the mixture solution *in vacuo*. The resultant product was cooled to room temperature and dissolved into 150 mL of diethyl ether anhydrous. The reaction mixture was washed with 5 wt % sodium bicarbonate (3 $\times$ 200 mL), and then washed with DI water (3 $\times$ 200 mL). The organic phase was dried with magnesium sulfate anhydrous (50 g). Solvent was removed *in vacuo* to give HD-SH as colorless oil. Yield, 23 g (85%). ^{1}H-NMR ($CDCl_3$): δ 1.38 ppm (m, 4H), 1.64 ppm (m, 6H), 2.63 ppm (t, 4H), 2.73 ppm (q, 4H), 4.09 ppm (t, 4H), ^{13}C-NMR ($CDCl_3$): δ 19.68, 25.44, 28.37, 38.35, 64.43, 171.46 ppm. FTIR (cm^{-1}, KBr plate): 2596 (s, SH stretching). Elemental analysis: carbon 63.38 wt %, hydrogen 9.51 wt %, oxygen 14.8 wt %, and sulfur 12.31 wt %. Calculated C, H, O, S content: carbon 60.54 wt %, hydrogen 8.71 wt %, oxygen 15.36 wt %, and sulfur 15.39 wt %.

Trans-1,4-cyclohexanedimethyl bis(3-mercaptopropionate)

trans-1,4-Cyclohexanedimethanol (14.08 g, 0.098 mol), 3-mercaptopropionic acid (23.84 g, 0.202 mol), and *p*-toluenesulfonic acid (0.2 g, 0.001 mol) were dissolved in toluene (150 mL) and charged into a 500-mL round-bottom three-necked flask equipped with mechanical stirrer, Dean-Stark trap, and reflux condenser. The mixture was purged with argon, and heated to reflux temperature $\sim$ 110°C. The mixture was kept at reflux temperature for 3 h to ensure completed reaction after which the toluene was removed from the mixture solution *in vacuo*. The resultant product was cooled to room temperature and dissolved into 150 mL of diethyl ether anhydrous. The reaction mixture was washed with 5 wt % sodium bicarbonate (3 $\times$ 200 mL), and then washed with DI water (3 $\times$ 200 mL). Organic phase was dried with magnesium sulfate anhydrous (50 g.). Solvent was removed *in vacuo* to give CHDM-SH as colorless oil. Yield, 26 g (80%). ^{1}H-NMR ($CDCl_3$): δ 0.99 ppm (m, 4H), 1.63 ppm (m, 4H), 1.94 ppm (d, 4H), 2.63 ppm (m, 4H), 2.73 ppm (m, 4H), 3.93 ppm (d, 4H), ^{13}C-NMR ($CDCl_3$): δ 19.58, 28.54, 36.73, 38.21, 69.20, 171.23 ppm. FTIR (cm^{-1}, KBr plate): 2596 (s, SH stretching). Elemental analysis: carbon 52.69 wt %, hydrogen 7.29 wt %, oxygen 20.06 wt %, and sulfur 19.96 wt %. Calculated C, H, O, S content: carbon 52.47 wt %, hydrogen 7.55 wt %, oxygen 19.97 wt %, and sulfur 20.01 wt %.

4,4′-Isopropylidenedicyclohexane bis(3-mercaptopropionate)

4,4′-Isopropylidenedicyclohexanol (25 g, 0.104 mol), 3-mercaptopropionic acid (26.05 g, 0.245 mol), and *p*-Toluenesulfonic acid (0.2 g, 0.001 mol) were dissolved in toluene (150 mL) and charged into a 500-mL round-bottom three-necked flask equipped with mechanical stirrer, Dean-Stark trap, and reflux condenser. The mixture was purged with argon, and heated to reflux temperature $\sim$ 110°C. The mixture was kept at reflux temperature for 10 h to ensure completed reaction after which the toluene was removed from the mixture solution *in vacuo*. The resultant product was cooled to room temperature and dissolved into 500 mL of diethyl ether anhydrous. The reaction mixture was washed with 5 wt % sodium bicarbonate (3 $\times$ 200 mL), and then washed with DI water (3 $\times$ 200 mL). The organic phase was dried with magnesium sulfate anhydrous (50 g). Solvent was removed *in vacuo* to give HBPA-SH as colorless oil. Yield, 32 g (75%). ^{1}H-NMR ($CDCl_3$): δ 0.72 ppm (m, 6H), 1.06–1.14 ppm (m, 4H), 1.22–1.30 ppm (m, 4H), 1.45–1.48 ppm (m, 2H), 1.59 ppm (m, 2H), 1.68–1.72 ppm (m, 4H), 2.56–2.65 ppm (m, 4H), 2.69–2.77 ppm (m, 4H), 4.59–4.69 ppm (m, 2H), ^{13}C-NMR ($CDCl_3$): δ 20.0, 20.68, 21.27, 24.89, 30.76, 32.27, 36.72, 38.89, 43.01, 70.05, 74.13, 171.18 ppm. FTIR (cm^{-1}, KBr plate): 2596 (s, SH stretching). Elemental analysis: carbon 49.40 wt %, hydrogen 7.53 wt %, oxygen 22.78 wt %, and sulfur 20.29 wt %. Calculated C, H, O, S content: carbon 48.95 wt %, hydrogen 7.53 wt %, oxygen 21.74 wt %, and sulfur 21.78 wt %.

Instrumentation and testing protocol

For characterization, ^{1}H-NMR and ^{13}C-NMR spectra were recorded on a Mercury-300 MHz spectrometer (Varian) in $CDCl_3$ as solvent at 20°C. Chemical shifts are given relative to a TMS internal standard.

TABLE I
Pseudo Formulation Matrix for Simplex Centroid Design of Experiments

Run	HD-SH	CHDM-SH	HBPA-SH
1	0.000	0.000	1.000
2	0.333	0.333	0.333
3	0.000	1.000	0.000
4	0.000	0.500	0.500
5	0.500	0.000	0.500
6	0.167	0.667	0.167
7	1.000	0.000	0.000
8	0.500	0.500	0.000
9	0.667	0.167	0.167
10	0.167	0.167	0.667

Fourier transform infrared spectroscopy (FTIR) was performed on an ATI Mattson Genesis FTIR spectrometer by the casting of thin liquid samples on KBr plates. Coatings were evaluated using the following tests: pencil hardness (D3363-74), pull-off adhesion (ASTM D 4541-85), and gloss. The mechanical properties were evaluated under ambient conditions.

The viscoelastic properties were investigated using a Perkin–Elmer Rheometric Scientific DMA in tension mode with a frequency of 1 Hz and heating rate of 5°C/min over a range of −100 to 150°C, an average sample thickness of 1 mm. The test geometry was rectangular ($10 \times 5 \times 1$ mm^3). The glass transition temperature (T_g) and the crosslink density (M_c or ν_e) were obtained from DMA analysis. The DMA spectrum has viscoelastic properties plotted versus temperature. The storage modulus and loss modulus measures the elastic and viscous response, respectively, of the material. The apex of the tan delta curve provides the T_g of the sample. The crosslink density (ν_e) is calculated from the storage modulus versus temperature plot using the following equation:

$$M_c \text{ or } v_e = E'_{\min}/3RT \quad (1)$$

where $E'_{\min}$ is minimum storage modulus, T (K) is temperature at minimum storage modulus, and R is the universal gas constant. The temperature and the minimum storage modulus data were obtained from the DMA spectrum.

The photopolymerization was measured by a Q1000 differential scanning calorimeter (TA instruments) equipped with a photocalorimeter accessory (PCA). The samples were placed in an aluminum pan at typically 3–5 mg. The intensity of the UV-light in the sample compartment was ~ 10 mW/cm^2. Polymerization was carried out in a nitrogen atmosphere at 25°C. The sample and reference were equilibrated at 25°C for 1 min. The shutter was opened, and the sample and reference pans were irradiated by UV light simultaneously for a given time. The sample was kept to re-equilibrate for 2 min. The resulting curves were analyzed with TA Instruments Universal Analysis software.

Tensile test were performed using Instron universal tester. Tensile properties, stress, strain, and tensile modulus were measured. The test was carried out at a strain rate 30 mm/min. The sample had an average width and thickness of 1.0 and 1.2 mm. An average of eight samples was tested for each composition, and the average values were recorded. A simplex centroid mixture design was created and analyzed by DESIGN-EXPERT@ software V.6 (Stat-Ease).

Formulations and film formation

The coatings formulations were statistically prepared according to the simplex centroid mixture with augment design as shown in Table I and depicted in Figure 2. The design mixture of three components has been chosen for the analysis and optimization of coatings formulations. The mixture in molar ratio of 1,6-Hexane bis(3-mercaptopropionate) (HD-SH), *trans*-1,4-Cyclohexanedimethyl bis(3-mercaptopropionate) (CHDM-SH), and 4,4′-isopropylidenedicyclohexane bis(3-mercaptopropionate) (HBPA-SH) was combined with 1,3,5-Triallyl-1,3,5-triazine-2,4,6(1*H*,3*H*,5*H*)-trione (TATATO) at 1 : 1 stoichiometric ratio (thiol : alkene). The photoinitiator was 1 wt % of the total formulation. Formulations were cast using a 150 μm (6 mil) draw down bar on aluminum panels for the coating test and formulations were prepared in 1-mm-thick glass mold to obtain the sample for the DMA and tensile test. Formulations were immediately placed in an ultraviolet processor (Fusion-system, medium-pressure mercury UV lamp at 5 fpm). After cure, the coatings were immediately

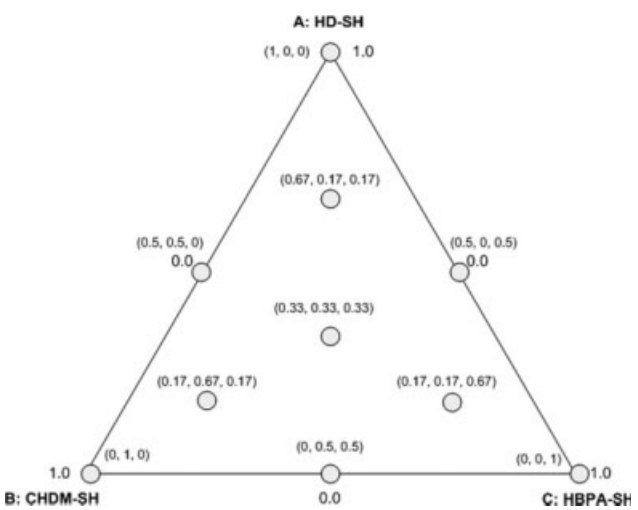

Figure 2 Simplex centroid design of experiment containing HD-SH, CHDM-SH, and HBPA-SH.

TABLE II
Tensile and Viscoelastic Properties

Run	Tensile strength (Mpa)	Tensile modulus (Mpa)	Elongation	T_g (°C)	XLD (mol/m^3)
1	7.592	114.57	1.02	74.2	442.23
2	2.114	5.69	0.75	46.1	653.81
3	2.246	6.79	0.65	7.3	867.17
4	4.024	21.36	1.82	60.3	756.30
5	1.881	4.65	0.82	44.2	598.65
6	1.934	5.30	0.62	40.4	788.53
7	0.728	5.14	0.20	38.7	1073.30
8	1.397	4.88	0.40	21.9	937.08
9	1.108	4.19	0.36	21.1	556.58
10	2.556	19.63	1.10	58.6	508.32

evaluated for dryness to touch. All testing was performed 7 days after curing.

RESULTS

In this study, three different chemical structures of mercaptopropionate thiol (HD-SH (linear), CHDM-SH (single cycloaliphatic), and HBPA-SH (double cycloaliphatic)) were chosen to evaluate the dependence of chemical structure on the material properties. 1,3,5-Triallyl-1,3,5-triazine-2,4,6(1*H*,3*H*,5*H*)-trione (TATATO) was chosen as a representative alkene and minimize the effect of homopolymerization. Utilization of experimental design is beneficial for optimization and investigation of interaction between parameters. In the previous study, the chemical structure and UV-curing reactivity of these three thiols was investigated.[10] The steric strain of cycloaliphatic structure causes the initial reaction rate and final conversion to be relatively lower than the linear structure. In this study, it should be anticipated that cycloaliphatic structure would provide hardness and higher glass transition temperature to the final cure film; although, steric strain lower the reactivity of the thiol.

Table II and III showed experimental results of each testing. Ten experimental runs according to simplex centroid design were completed. Experimental data shown in Table II and III were analyzed by DESIGN-EXPERT@ software V.6 (Stat-Ease). Summary of ANOVA and statistical results is shown in Table IV and V.

The results are shown in ternary contour plots that are a simplification of the three-dimensional model shown in Figure 3. The minimum of three-dimensional model is at the two vertices and the maximum is at the other vertex. This model is an attempt to fit a mathematical model surface that connects the four points from the test results. The contours trace the surface of the three-dimensional model at a given value. Using this method, trends of properties can be quickly established. Locating peaks and valleys along the contour correlates to synergistic or antagonistic results. In addition, overlay of the plots enable rapid target formulation of certain properties by locating regions where the desired properties overlap.

The ternary plot in Figure 4(a) shows linearly improved tensile strength with increasing the molar concentration of HBPA-SH ranging from 1 to 5 MPa The tensile strength also increases with the molar concentration of CHDM-SH ranging from 1 to 2 MPa without HBPA-SH. The minimum tensile strength occurs with the pure HD-SH formulation. The data in Figure 4 were obtained from the statistical calculation. A linear model relationship between HD-SH, CHDM-SH, and HBPA-SH was selected. The best fit mathematical model in term of actual component for the tensile strength is

$$\text{Tensile strength} = -0.08733 \times (\text{HD-SH}) + 1.91433 \times (\text{CHDM-SH}) + 5.84700 \times (\text{HBPA-SH}) \quad (2)$$

The model *F*-value of 11.83 implies that the model is significant. There is only a 0.57% chance that a *F*-value this large could occur due to the noise. Values of prob. $> F$ less than 0.0500 indicate that the model terms are significant. In this case, linear mixture component are significant model terms. Values greater than 0.1000 indicate the model terms are not significant. Other statistics of interest are the

TABLE III
General Coatings Properties and Heat of Reaction

Run	Gloss 20°	Gloss 60°	Pencil hardness	Pull-off adhesion	MEK double rub	Heat of reaction (J/g)
1	161.1	167.9	3H	200	>500	239.1
2	190.1	172.4	2H	200	>500	327.7
3	190.4	170.8	2H	210	>500	350.5
4	135.3	171.2	2H	250	>500	317.9
5	189.0	174.6	H	200	>500	324.2
6	182.4	170.3	2H	210	>500	360.8
7	185.1	170.2	HB	100	>500	378.7
8	190.1	173.5	F	100	>500	375
9	188.5	173.9	HB	110	>500	367.5
10	169.3	170.1	2H	250	>500	297.0

TABLE IV
Summary of ANOVA and Statistical Values

	Tensile strength	Tensile modulus	Elongation	XLD	T_g
Fit model	Linear	Quadratic	Special cubic	Linear	Linear
F-value	11.83	22.7	19.17	6.87	12.91
Standard deviation	1.07	9.44	0.13	133.09	10.65
Mean	2.56	19.22	0.77	718.2	41.28
R-square	0.7717	0.966	0.9746	0.6625	0.7868
Adj *R*-square	0.7065	0.9234	0.9238	0.566	0.7258
PRESS	25.19	7202.37	1.35	3.19×10^5	2088.78
Adeq-precision	10.08	15.417	14.59	6.819	9.962

following: standard deviation = 1.07, *R*-squared = 0.7717, mean = 2.56, adj *R*-squared = 0.7065, PRESS = 25.19, adeq precision = 10.080. The Adeq precision measures the signal-to-noise ratio. A ratio greater than 4 is desirable. The ratio in Figure 4 of 10.080 indicates an adequate signal. This model can be used to navigate the design space.

In Figure 5, the ternary plots representing of tensile modulus results are shown. The plot shows improved of tensile modulus with increasing the concentration of HBPA-SH ranging from 10 to 90 MPa. The maximum of tensile modulus appears at the apex of HBPA-SH. The HD-SH and CHDM-SH mixture shows no synergistic effect on tensile modulus. The data in Figure 5 were fit with a quadratic model. The model *F*-value of 22.70 implies the model is significant. This model can be used to navigate the design space. ANOVA and other statistical of interests are listed in Table IV and V. The final equation in terms of actual components is:

$$\begin{aligned}\text{Tensile Modulus} &= 7.46934 \times (\text{HD-SH}) + 7.75398 \\ &\times (\text{CHDM-SH}) + 109.66534 \times (\text{HBPA-SH}) \\ &+ 9.65442 \times (\text{HD-SH}) \times (\text{CHDM-SH}) \\ &- 218.58285 \times (\text{HD-SH}) \times (\text{HBPA-SH}) \\ &- 157.78158 \times (\text{CHDM-SH}) \times (\text{HBPA-SH}) \quad (3)\end{aligned}$$

As shown in Figure 6, elongation-to-break trend is clearly shown. The maximum of elongation is located between HBPA-SH and CHDM-SH (~ 180%) and the minimum is on the HD-SH vertex (~ 18%). The HBPA-SH quadrants also display a relatively higher elongation than the other two. The combination of HBPA-SH and CHDM-SH showed a strong synergistic effect on improving elongation-to-break. The elongation-to-break data in Figure 6 were fit with a special cubic model. The model *F*-value of 19.17 implies the model is significant. This model can be used to navigate the design space. ANOVA and other statistical of interests are listed in Table IV and V. The final equation in term of actual components is:

$$\begin{aligned}\text{Elongation to break} &= 0.21437 \times (\text{HD-SH}) \\ &+ 0.60019 \times (\text{CHDM-SH}) + 1.02601 \\ &\times (\text{HBPA-SH}) - 0.19887 \times (\text{HD-SH}) \\ &\times (\text{CHDM-SH}) + 0.86476 \times (\text{HD-SH}) \\ &\times (\text{HBPA-SH}) + 3.86040 \times (\text{CHDM-SH}) \\ &\times (\text{HBPA-SH}) - 12.52059 \times (\text{HD-SH}) \\ &\times (\text{CHDM-SH}) \times (\text{HBPA-SH}) \quad (4)\end{aligned}$$

The glass transition temperature model is shown in Figure 7. The result shows clearly an increase in the T_g with increasing concentration of HBPA-SH. The maximum value of T_g appears at the apex of HBPA-SH (~ 75°C), whereas the minimum showed at the apex of CHDM-SH (~ 20°C). The glass transition temperature data in Figure 7 were fit with a

TABLE V
Summary of ANOVA and Statistical Values (Cont.)

	Gloss 20°	Gloss 60°	Pencil hardness	Pull-off adhesion	Heat of reaction
Fit model	Special cubic	Quadratic	Linear	Quadratic	Linear
F-value	29.11	3.02	25.08	14.32	71.21
Standard deviation	4.06	1.42	0.55	20.06	10.53
Mean	178.13	171.48	11.2	183	333.84
R-square	0.9831	0.7906	0.8775	0.9471	0.9531
Adj *R*-square	0.9493	0.5288	0.8425	0.881	0.9398
PRESS	1700.74	118.23	3.63	33271.89	2459.98
Adeq-precision	16.971	5.52	14.257	11.204	23.515

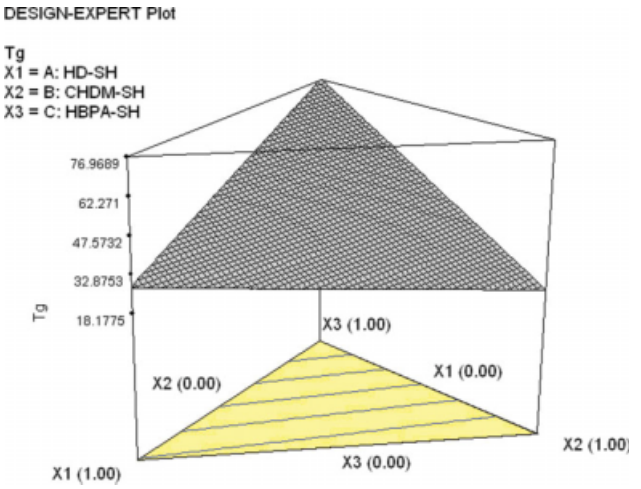

Figure 3 Three-dimensional surface plot for glass transition temperature. [Color figure can be viewed in the online issue, which is available at www.interscience.wiley.com.]

linear model. The model *F*-value of 12.91 implies the model is significant. This model can be used to navigate the design space. ANOVA and other statistical of interests are listed in Table IV and V. The final equation in terms of actual components is:

$$T_g = 28.00222 \times (\text{HD-SH}) + 18.86889 \times (\text{CHDM-SH}) + 76.96889 \times (\text{HBPA-SH}) \quad (5)$$

The crosslink density (XLD) model calculation is shown in Figure 8. There is a clear trend showing that XLD decrease with the concentration of HBPA-SH and reach the minimum at the apex of HBPA-SH ($\sim$ 440 mol/m^3). The maximum of XLD locates at the vertex of HD-SH ($\sim$ 1070 mol/m^3). It should be noted that the XLD of CHDM-SH shows slightly different from HD-SH at the same level of HBPA-SH. The XLD data in Figure 8 were fit with a linear model. The model *F*-value of 6.87 implies the model is significant. ANOVA and other statistical of interests are listed in Table IV and V. This model can be used to navigate the design space. The final equation in terms of actual components is:

$$\text{XLD} = 886.40314 \times (\text{HD-SH}) + 878.84592 \times (\text{CHDM-SH}) + 389.34158 \times (\text{HBPA-SH}) \quad (6)$$

The ternary plots in Figures 9 and 10 show the model of 20° gloss and 60° gloss. 20° Gloss shows the minimum at the local between HBPA-SH and CHDM-SH but the minimum is favored to the side of CHDM-SH. As the concentration of HD-SH increases, 20° gloss appears to be increasing and reach the maximum. However, 20° gloss slightly decreases when approaching to the apex of HBPA-SH. For 60° gloss, the trend appears to be in the same manner as 20° gloss. 60° Gloss shows low value at the apex of the three components. A synergistic effect between HBPA-SH and HD-SH creates the maximum 60° gloss. Some synergistic effect

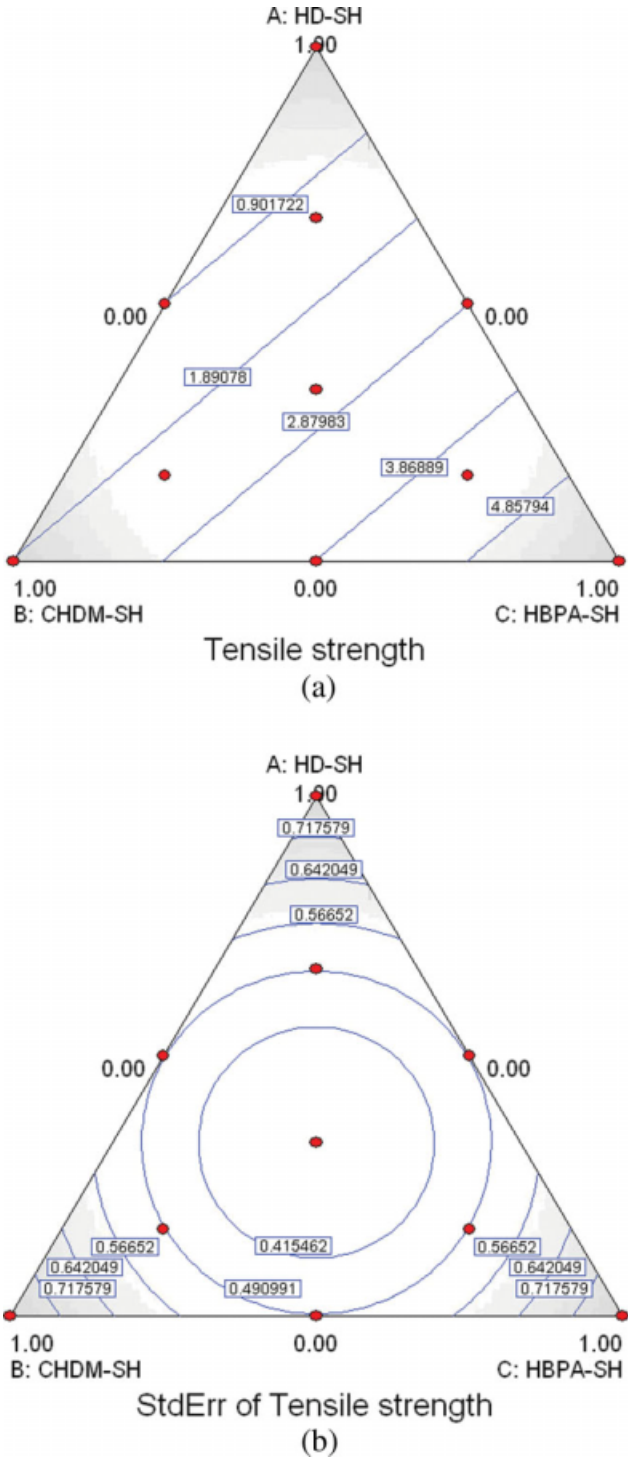

Figure 4 Contour plot of tensile strength model (a) and standard error (b). [Color figure can be viewed in the online issue, which is available at www.interscience.wiley.com.]

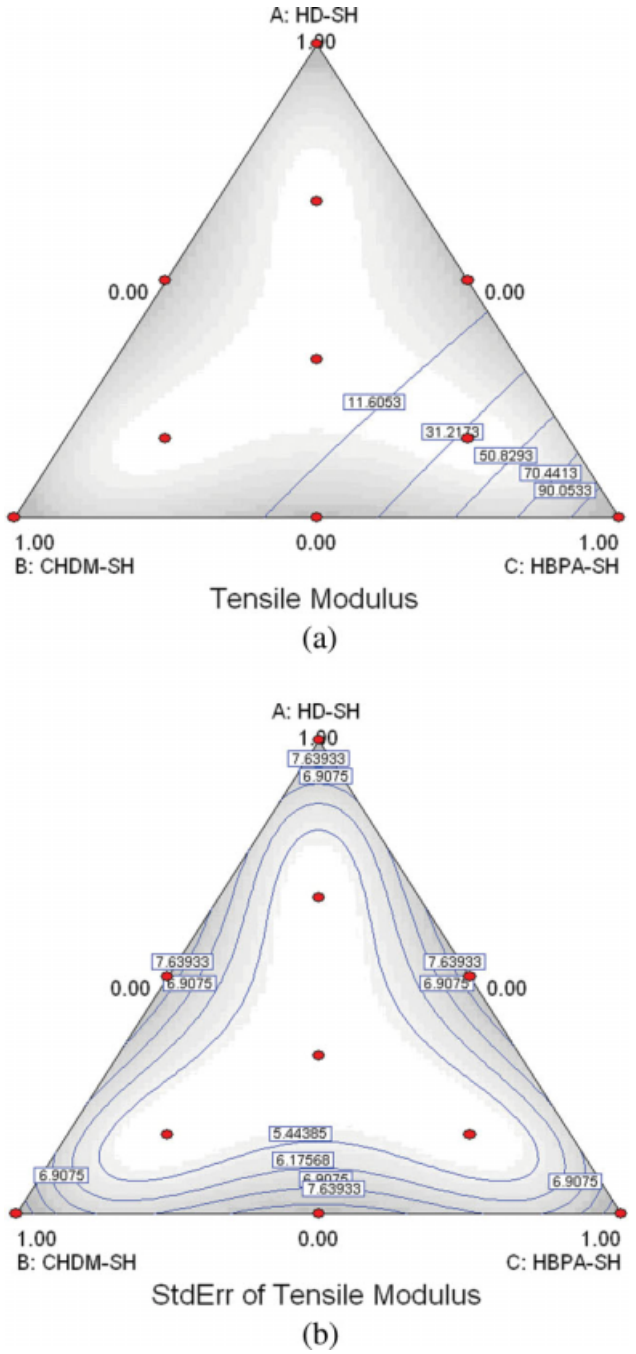

Figure 5 Contour plot of tensile modulus model (a) and standard error (b). [Color figure can be viewed in the online issue, which is available at www.interscience.wiley.com.]

between CHDM-SH and HD-SH can be observed in the model.

The data in Figure 9 were fit with special cubic model. The Model *F*-value of 29.11 implies the model is significant. This model can be used to navigate the design space. ANOVA and other statistical of interests are listed in Table IV and V. The final equation in terms of actual components is:

$$\begin{aligned} 20^{\circ}\text{Gloss} = {} & 183.37340 \times (\text{HD-SH}) + 191.40976 \\ & \times (\text{CHDM-SH}) + 161.30067 \times (\text{HBPA-SH}) \\ & + 7.96631 \times (\text{HD-SH}) \times (\text{CHDM-SH}) \\ & + 60.54813 \times (\text{HD-SH}) \times (\text{HBPA-SH}) \\ & - 159.37914 \times (\text{CHDM-SH}) \times (\text{HBPA-SH}) \\ & + 538.72941 \times (\text{HD-SH}) \\ & \times (\text{CHDM-SH}) \times (\text{HBPA-SH}) \end{aligned} \quad (7)$$

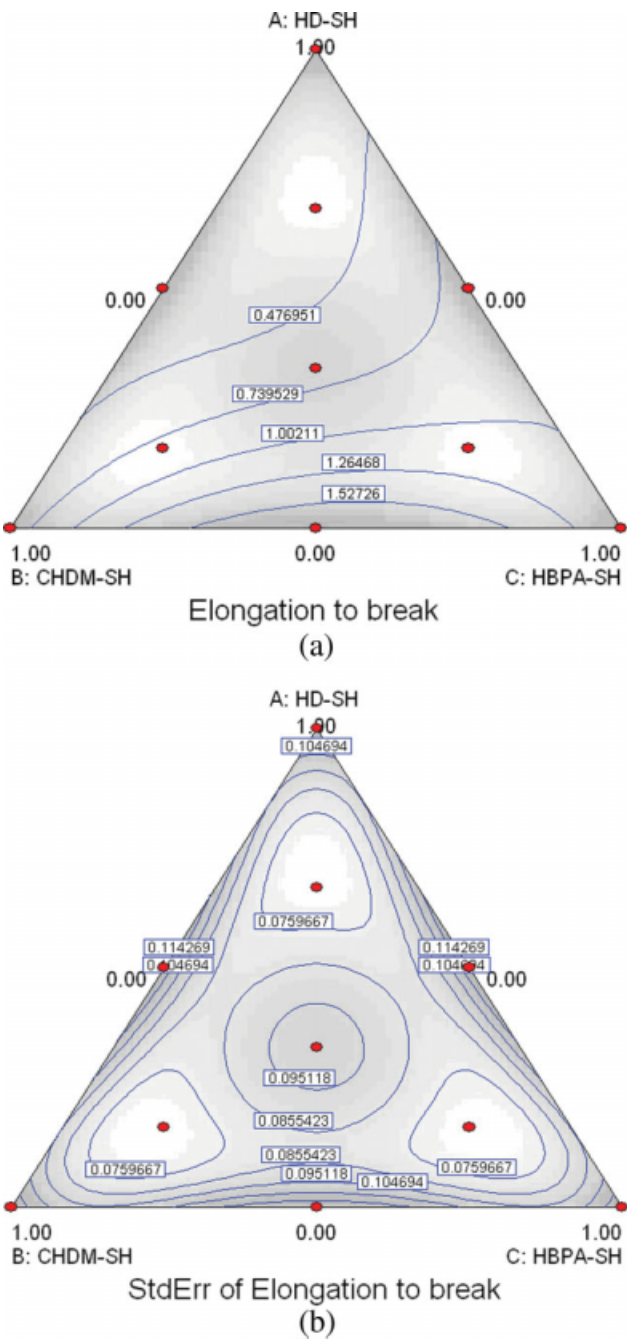

Figure 6 Contour plot of elongation-to-break model (a) and standard error (b). [Color figure can be viewed in the online issue, which is available at www.interscience.wiley.com.]

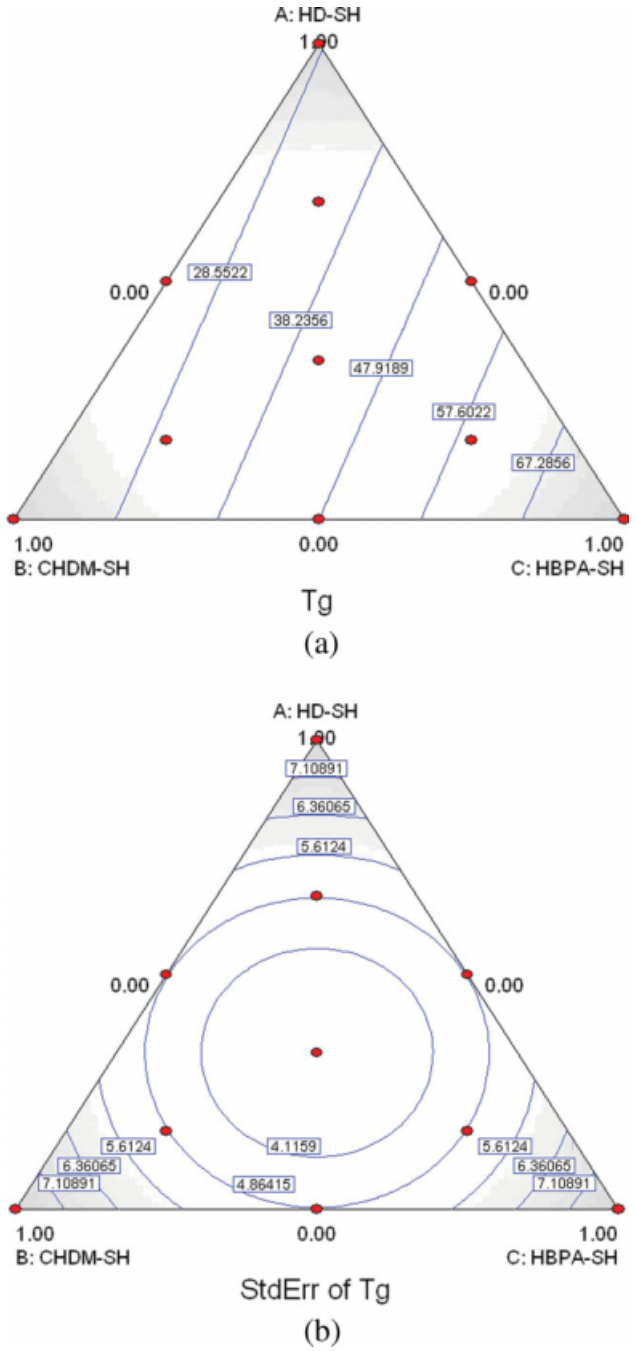

Figure 7 Contour plot of glass transition temperature model (a) and standard error (b). [Color figure can be viewed in the online issue, which is available at www.interscience.wiley.com.]

The data in Figure 10 were fit with quadratic model. The model *F*-value of 3.02 implies the model is not significant relative to the noise. This model can be used to navigate the design space. ANOVA and other statistical of interests are listed in Table IV and V. The final equation in terms of actual components is:

$$\begin{aligned} 60^{\circ}\text{Gloss} &= 170.73930 \times (\text{HD-SH}) + 170.52930 \\ &\times (\text{CHDM-SH}) + 167.82112 \times (\text{HBPA-SH}) \\ &+ 8.27869 \times (\text{HD-SH}) \times (\text{CHDM-SH}) \\ &+ 18.46232 \times (\text{HD-SH}) \times (\text{HBPA-SH}) \\ &+ 2.44232 \times (\text{CHDM-SH}) \times (\text{HBPA-SH}) \end{aligned} \quad (8)$$

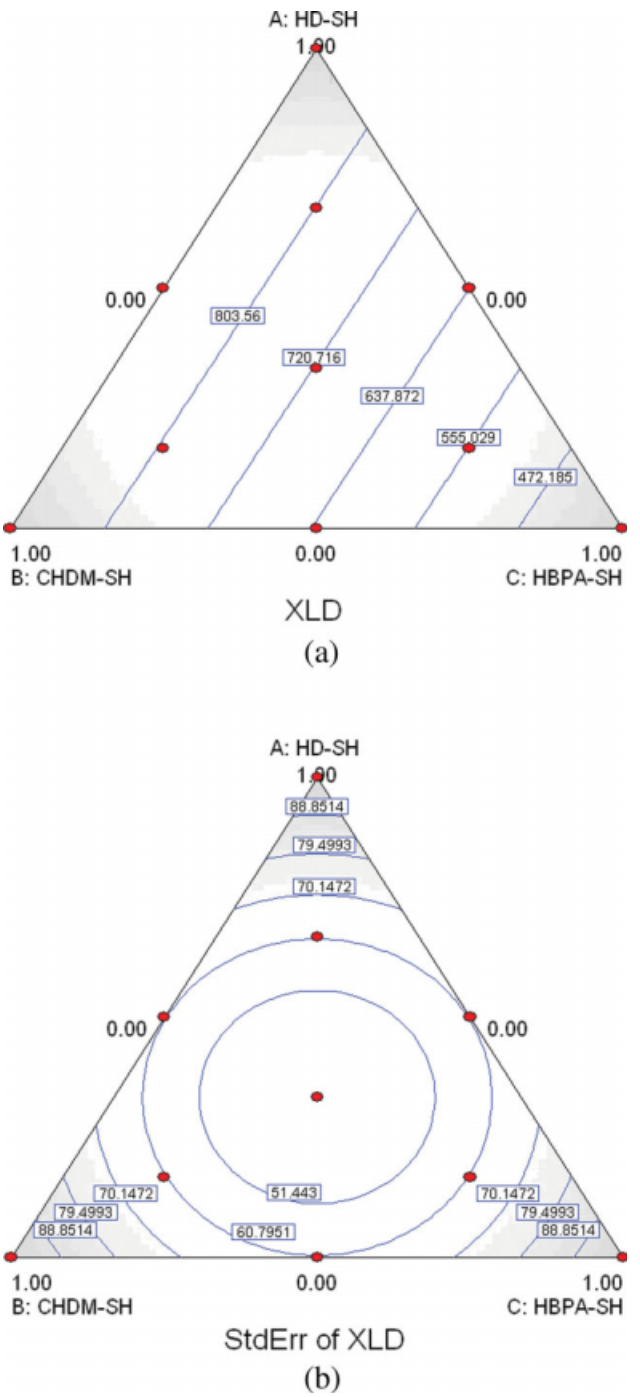

Figure 8 Contour plot of XLD (v_e) model (a) and standard error (b). [Color figure can be viewed in the online issue, which is available at www.interscience.wiley.com.]

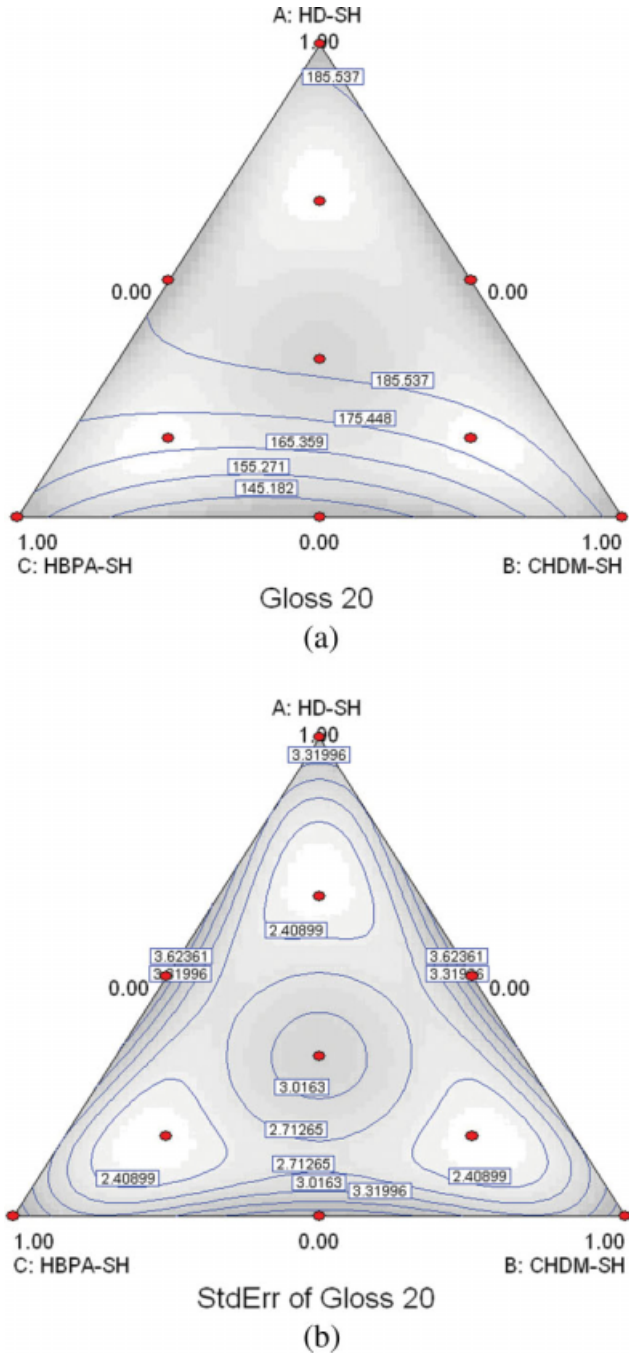

Figure 9 Contour plot of gloss 20° model (a) and standard error (b). [Color figure can be viewed in the online issue, which is available at www.interscience.wiley.com.]

In Figure 11, the ternary plots representing of pencil hardness results are shown. Pencils 8B-B, HB, F, and H-9H were assigned a respective number from 1 to 19 from soft to hard graphite, respectively. There is a trend of increased hardness toward both CHDM-SH and HBPA-SH apexes in the range of a pencil hardness of 2H to 3H. There is also increase in hardness for the points located near the HBPA-SH vertex. The minimum hardness appears at the apex of HD-SH. The data in Figure 11 were fit with linear model. The model *F*-value of 25.08 implies the model is significant. This model can be used to navigate the design space. ANOVA and other statistical of interests are listed in Table IV and V. The final equation in terms of actual components is:

$$\text{Hardness} = 8.64444 \times (\text{HD-SH}) + 11.97778 \times (\text{CHDM-SH}) + 12.97778 \times (\text{HBPA-SH}) \quad (9)$$

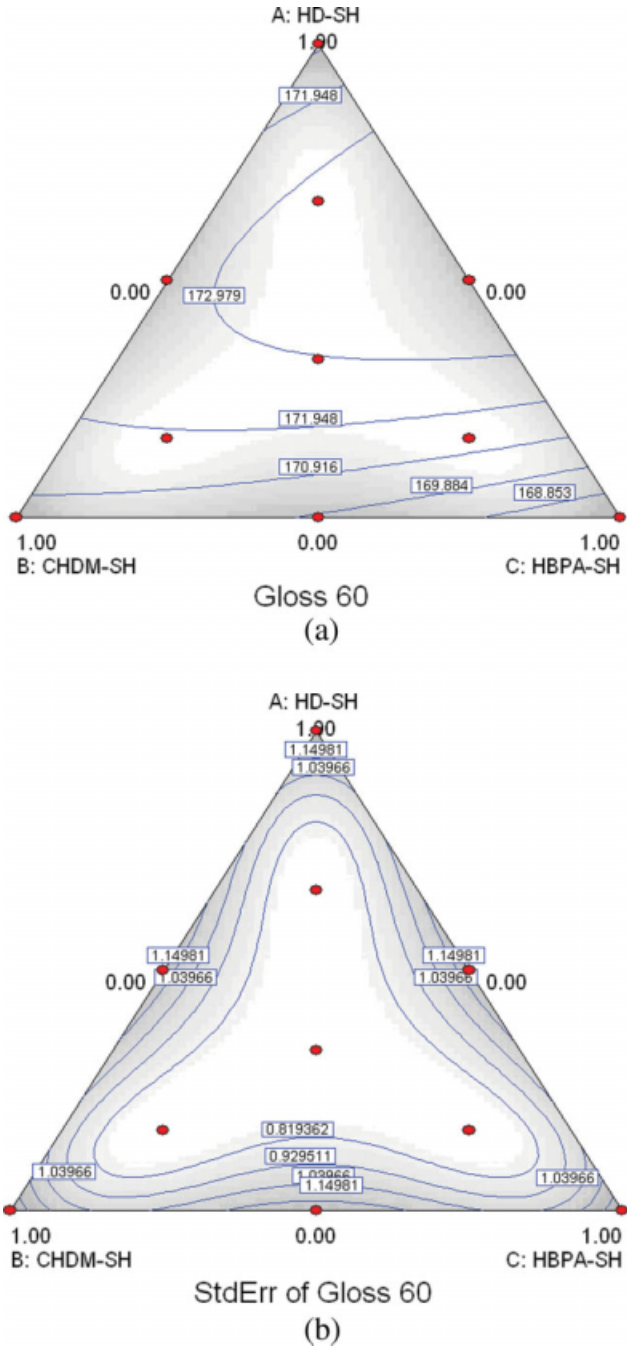

Figure 10 Contour plot of gloss 60° model (a) and standard error (b). [Color figure can be viewed in the online issue, which is available at www.interscience.wiley.com.]

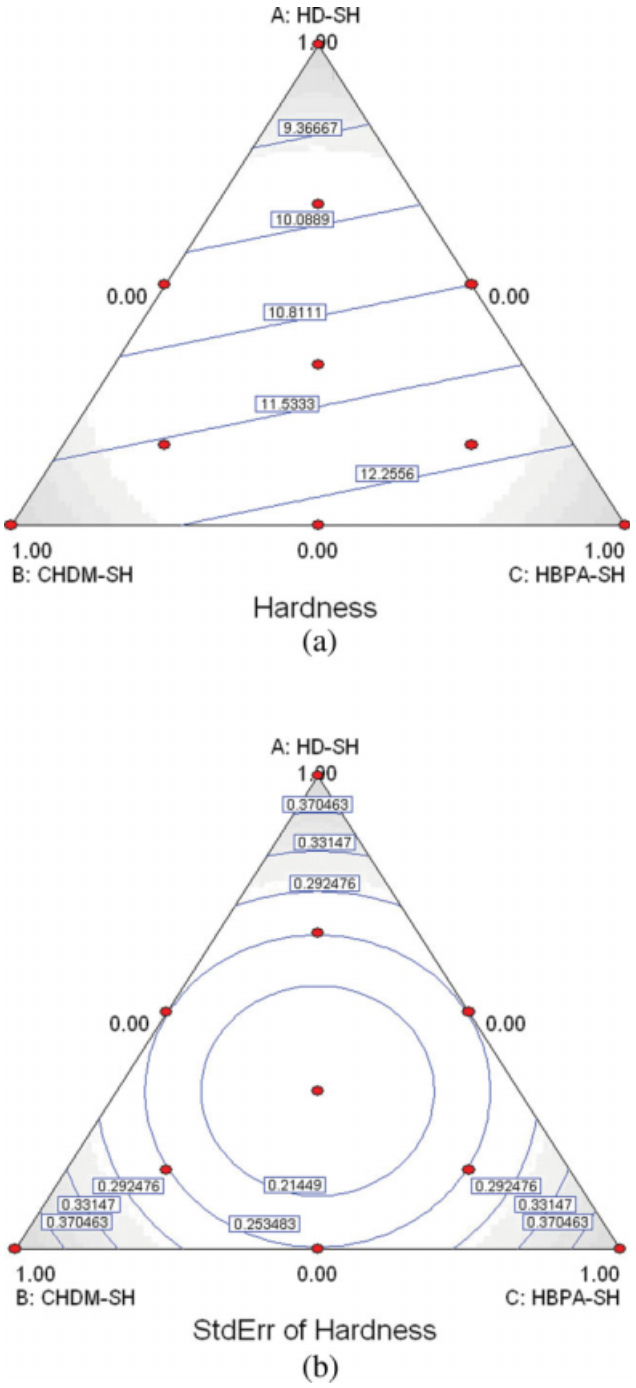

Figure 11 Contour plot of hardness model (a) and standard error (b). [Color figure can be viewed in the online issue, which is available at www.interscience.wiley.com.]

Pull-off adhesion can be seen in Figure 12. A synergistic effect between HBPA-SH and CHDM-SH gives the maximum adhesion between these two components and giving the adhesive strength up to 260 lb/in.^{2} The lowest value (100 lb/in^2) is located at the HD-SH apex. The pull-off adhesion data in Figure 12 were fit with quadratic model. The model *F*-value of 14.32 implies the model is significant. This model can be used to navigate the design space. ANOVA and other statistical data of interests are listed in Table IV and V. The final equation in terms of actual components is:

$$\begin{aligned}\text{Adhesion} = {} & 89.95791 \times (\text{HD-SH}) + 212.68519 \\ & \times (\text{CHDM-SH}) + 205.41246 \times (\text{HBPA-SH}) \\ & - 211.01010 \times (\text{HD-SH}) \times (\text{CHDM-SH}) \\ & + 214.44444 \times (\text{HD-SH}) \times (\text{HBPA-SH}) \\ & + 219.89899 \times (\text{CHDM-SH}) \times (\text{HBPA-SH}) \quad (10)\end{aligned}$$

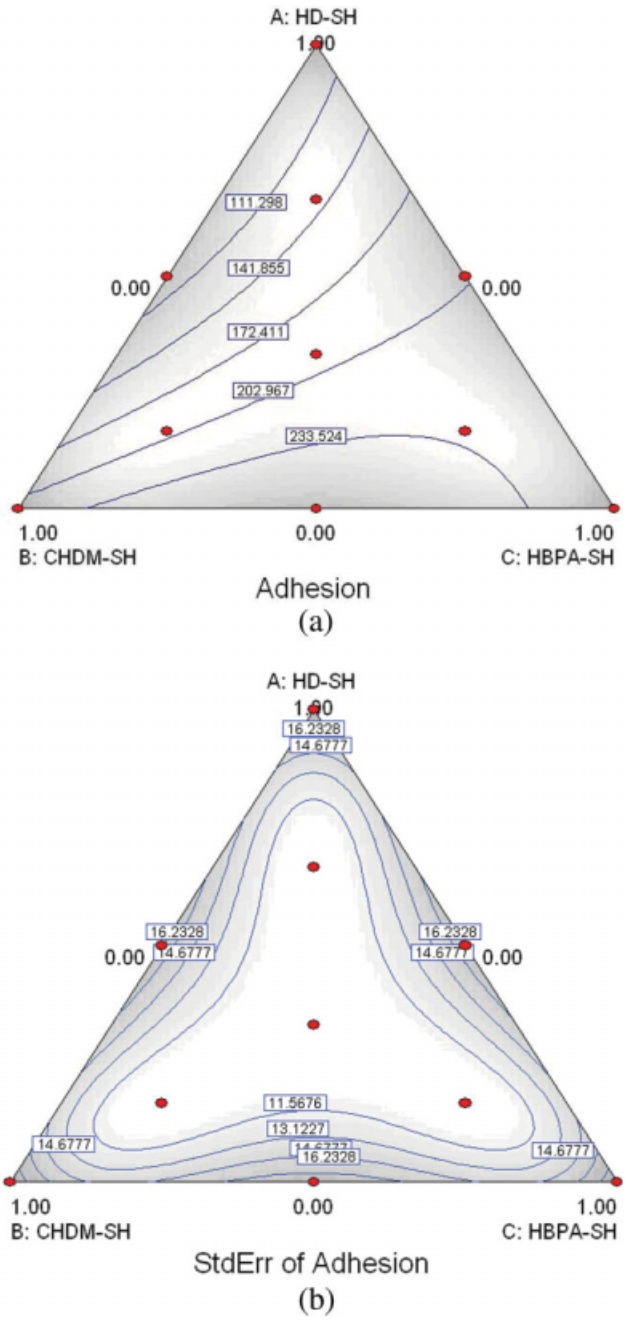

Figure 12 Contour plot of adhesion model (a) and standard error (b). [Color figure can be viewed in the online issue, which is available at www.interscience.wiley.com.]

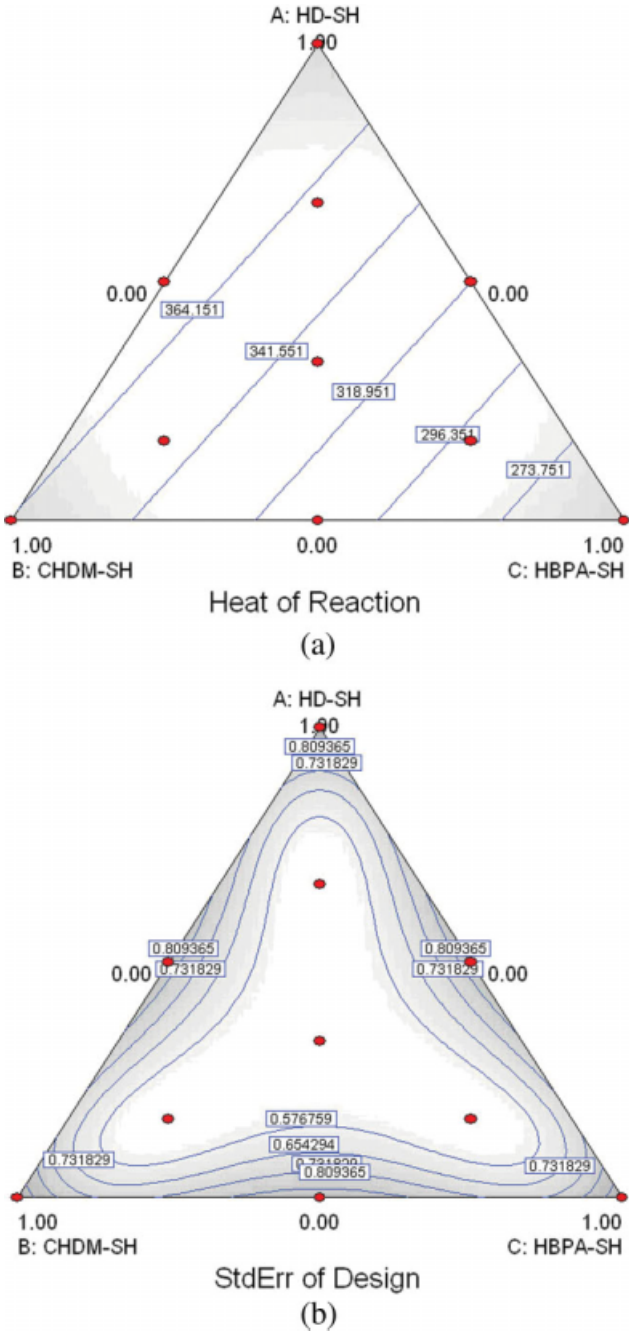

Figure 13 Contour plot of heat of reaction model (a) and standard error (b). [Color figure can be viewed in the online issue, which is available at www.interscience.wiley.com.]

The heat of reaction model is shown in Figure 13. The result clearly showed that increasing the concentration of HBPA-SH suppressed the heat of reaction or the conversion of monomer. The maximum heat of reaction appeared at the apex of HD-SH (378.3 J/g), whereas the minimum showed at the apex of HBPA-SH (237.1 J/g). The heat of reaction data in Figure 13 were fit with a linear model. The model *F*-value of 71.21 implied the model is significant. This model can be used to navigate the design space. ANOVA and other statistical of interests are listed in Table IV and V. The final equation in terms of actual components is:

$$\begin{aligned}\text{Heat of Reaction (J/g)} &= 386.75111 \times (\text{HD-SH}) \\ &+ 363.61778 \times (\text{CHDM-SH}) \\ &+ 251.15111 \times (\text{HBPA-SH}) \quad (11)\end{aligned}$$

DISCUSSION

One of the objectives of this study was to investigate synergistic effect on the coatings properties of the three mercaptopropionate thiols, HD-SH, CHDM-SH, and HBPA-SH for thiol-ene photopolymerization by utilizing the statistical evaluation. It should be noted that the coatings properties of thiol-ene photopolymerization materials have not been previously reported, so, this study can be considered as a benchmarking study. Binary system of thiol-ene-ene (two alkenes) and thiol-ene/acrylates (two alkenes) has been studied to tailor the final properties of the thiol-ene materials,[11,13] whereas in this study, a ternary system of thiols was used. Another objective was to reveal the effect of the particular mercaptopropionate thiol on thermal, mechanical, and coatings properties.

Three statistical scenarios were found. The first category was no problem in error and fit with good usable design space meaning that the results predictive design space was dependable. Pencil hardness and heat of reaction resided in this category. The second category was a problem in error and fit, yet having a usable design space. This was attributed to a large block effect that had some effect on the overall model fit. Six material properties: tensile strength, tensile modulus, elongation-to-break, crosslink density glass transition temperature, and 20° gloss fell into this category. The final category is where the mean was a better prediction than the statistical model, and this was the case for pull-off adhesion and 60° gloss.

Because of the inherently variation of the chemical structure of the three thiols, HD-SH (linear), CHDM-SH (single-cycloaliphatic), HBPA-SH (double-cycloaliphatic), combination of these thiols would expect to afford a wide range of mechanical and coatings properties. The glass transition temperature, tensile strength, tensile modulus as expected, increases with the concentration of HBPA-SH. Improvement of pencil hardness can also be anticipated with the amount of HBPA-SH incorporated into the system. The phenomena were attributed from the double-cycloaliphatic structure from HBPA-SH providing the rigidity and toughness the materials. On the other hand, crosslink density (XLD) and heat of reaction (relative

conversion), as expected, reduce proportionally to the concentration of HBPA-SH. Even though CHDM-SH (single-cycloaliphatic) exhibits some steric and rigidity, the HD-SH and CHDM-SH provide approximately the same XLD amount and more complete reaction. The HBPA-SH is by far more sterically hindered and rigid than the other two thiols, which is in agreement with a previous kinetics study.[10] The flexible HD-SH caused higher completion of reaction (ponderal effect) and resulted in higher crosslink density.

Synergistic effect was found in the elongation-to-break, pull-off adhesion, 20° gloss and 60° gloss; hence, the optimum values were obtained from a binary or ternary system. Maximum elongation-to-break exhibits in the binary mixture of HBPA-SH and CHDM-SH. Rigidity and toughness of HBPA-SH combined with high crosslink density of CHDM-SH resulted in an optimum elongation-to-break. Pull-off adhesion reveals the synergistic effect of HBPA-SH and CHDM-SH as well. The best adhesion can be observed with the mixture of the two thiols, while HD-SH (alone) shows inferior adhesion to the aluminum substrate. The gloss, both 20° and 60°, shows a synergistic result with the maximum gloss for the combination of three thiols with a maximum near the HD-SH apex.

In thiol-ene photopolymerization, there are a number of available thiols and alkenes, which can be combined to give a unique material property. It is difficult to find the best combination of thiols and alkenes without a systematic method of study. By and large, the statistical design did reveal both synergistic and antagonistic relationships between variables and showed the ability to achieve the optimum and predictive results with the minimum set of experiments. Therefore, statistical design was beneficial in with respect to studying thiol-ene photopolymerization as end usage coatings. As a formulation guide, the cyclohexyl based thiols provided hardness, tensile strength, T_g, and chemical resistance. The acyclic HD-SH provides flexibility, toughness, and completeness of cure to balance out the rigidity of the cyclohexyl groups (or aromatic groups for that matter).

Thiol-ene photopolymerization has shown large potential in coatings application, but there is no previous literature that reported the coatings properties of thiol-ene photopolymerization coatings. In comparison to other coatings system such as oil-based ceramer coatings,[14] polyacrylate[15] and polyurethane,[16] thiol-ene photopolymerization coatings performs comparable hard film (pencil hardness), good solvent resistance, and high gloss while providing more flexibility to the coating film. In UV-curing system, as mentioned earlier, thiol-ene UV-curable coatings posses the distinct advantages including no oxygen inhibited, delayed gelation, low shrinkage, high conversion, and uniform crosslink density.

CONCLUSIONS

A statistical approach to formulate and evaluate the material was accomplished. The HBPA-SH rich formulation resulted in improved tensile strength, tensile modulus, glass transition temperature and pencil hardness. Crosslink density and heat of reaction (relative conversion) decrease with HBPA-SH content due to the steric and rigidity of the double cycloaliphatic structure. A synergistic effect of CHDM-SH and HBPA-SH resulted an improving of elongation-to-break and pull-off adhesion was observed. The HD-SH improved the crosslink density due to the freedom of motion (flexibility) which led to more termination.

References

1. Pappas, S. P. Radiation Curing: Science and Technology; Plenum Press: New York, 1992; p 448.
2. Fouassier, J.-P. Photoinitiation, Photopolymerization, and Photocuring: Fundamentals and Applications; Hanser/Garner Publications, Inc.: Cincinnati, OH, 1995; p 338.
3. Hoyle, C. E. J Polym Sci A: Polym Chem 2004, 42, 5301.
4. Posner, T. Ber Dtsch Chem Ges 1905, 38, 646.
5. Morgan, C. R.; Ketley, A. D. J Polym Sci Polym Lett Ed 1978, 16, 75.
6. Gush, D. P.; Ketley, A. D. Mod Paint Coat 1978, 68, 58.
7. Fouassier, J.-P.; Rabek, J. F. Polym Mech 1993, 3, 453.
8. Jacobine, A. F. Radiat Curing Polym Sci Technol 1993, 3, 219.
9. Senyurt, A. F.; Wei, H.; Phillips, B.; Cole, M.; Nazarenko, S.; Hoyle, C. E.; Piland, S. G.; Gould, T. E. Macromolecules 2006, 39, 6315.
10. Wutticharoenwong, K.; Soucek, M. Macro Mat Eng 2008, 293, 45.
11. Lee, T. Y.; Smith, Z.; Reddy, S. K.; Cramer, N. B. Macromolecules 2007, 40, 1466.
12. Myers, R. H.; Montgomery, D. C. Response Surface Methodology, Process and Product Optimization Using Designed Experiments, 2nd ed.; Wiley: New York, 2002.
13. Wei, H.; Senyurt, A. F.; Jonsson, S.; Hoyle, C. E. J Polym Sci A: Polym Chem 2007, 45, 822.
14. Tuman, S. J.; Soucek, M. D. J Coat Technol 1996, 68, 73.
15. Park, H.-S.; Yang, I.-M.; Wu, J.-P.; Kim, M.-S.; Hahm, H.-S.; Kim, S.-K; Rhee, H. W. J Appl Polym Sci 2001, 81, 1614.
16. Gooch, J. W.; Dong, H.; Schork, F. J. J Appl Polym Sci 2000, 76, 105.